ACS ENGINEERING Au
AN OPEN ACCESS JOURNAL OF THE AMERICAN CHEMICAL SOCIETY

pubs.acs.org/engineeringau

Article

Interrogation of the Plasma-Catalyst Interface via In Situ/Operando Transmission Infrared Spectroscopy

Russell J. Clarke and Jason C. Hicks*

Cite This: *ACS Eng. Au* 2022, 2, 535−546

Read Online

ACCESS | Metrics & More | Article Recommendations

ABSTRACT: Plasma-surface coupling has emerged as a promising approach to perform chemical transformations under mild conditions that are otherwise difficult or impossible thermally. However, a few examples of inexpensive and accessible *in situ/operando* techniques exist for observing plasma-solid interactions, which has prevented a thorough understanding of underlying surface mechanisms. Here, we provide a simple and adaptable design for a dielectric barrier discharge (DBD) plasma cell capable of interfacing with Fourier transform infrared spectroscopy (FTIR), optical emission spectroscopy (OES), and mass spectrometry (MS) to simultaneously characterize the surface, the plasma phase, and the gas phase, respectively. The system was demonstrated using two example applications: (1) plasma oxidation of primary amine functionalized SBA-15 and (2) catalytic low temperature nitrogen oxidation. The results from application (1) provided direct evidence of a 1% O_2/He plasma interacting with the aminosilica surface by selective oxidation of the amino groups to nitro groups without altering the alkyl tether. Application (2) was used to detect the evolution of NO_X species bound to both platinum and silica surfaces under plasma stimulation. Together, the experimental results showcase the breadth of possible applications for this device and confirm its potential as an essential tool for conducting research on plasma-surface coupling.

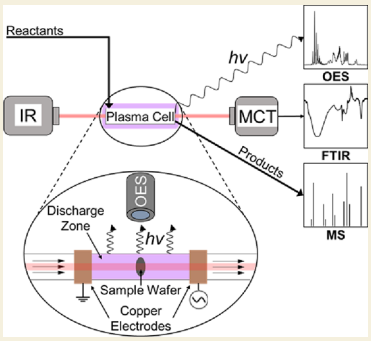

KEYWORDS: *nonthermal plasma, plasma-catalysis, in situ, operando, transmission FTIR, aminosilica oxidation, N_2 oxidation*

1. INTRODUCTION

Non-thermal plasmas (NTPs) are partially ionized gases characterized by a non-equilibrium in temperature between high energy electrons (>10,000 K) and low energy ions and neutrals (∼ambient temperature).[1] The energetic electrons are the primary driver for promoting gas-phase and/or surface reactions through collisions with neutral gas-phase molecules to form electronically, vibrationally, and rotationally excited species as well as radicals that react with increased activity over ground-state species[2] and surfaces to induce morphological or chemical changes (e.g., sputtering or etching).[3] These excited species can further collide with other gas-phase species to form high energy mixtures of electrons, ions, radicals, excited species, metastables, and photons while maintaining a bulk-gas temperature near ambient.[2]

Low-temperature plasma-induced interactions have been exploited for a wide range of applications including medical treatments,[4−7] pollutant removal,[8,9] electronics manufacturing,[5,10] material synthesis,[2,5,11−16] and heterogeneous catalysis.[2,17−24] Plasma-assisted catalysis has seen a significant growth in research activity over the past decade, primarily motivated by the ability to activate stable molecules (e.g., CH_4,[23,25−29] CO_2,[23,25−27,29−32] and N_2[22,33−38]) at relatively low temperature through electrical energy input. However, the complexity of plasma-phase interactions with reactive surfaces has resulted in many empirical studies on the performance of different catalytic materials with limited information on the fundamental elementary processes occurring at the plasma−catalyst interface.[2,21] Therefore, a transition toward *operando* and *in situ* characterization approaches can advance the field by directly observing how plasma stimulation affects the evolution of surface speciation. Of additional importance is the need for simple and inexpensive plasma modules capable of interfacing with existing and commonly utilized *in situ/operando* characterization techniques. Wide access to these systems provides researchers with a tool to correlate product output with time-resolved characterization of both the catalyst surface and the plasma phase.

Recent progress in this area has largely focused on identifying adsorbates on a metal surface under plasma stimulation and correlating plasma input conditions with observations. For plasma-assisted catalytic ammonia synthesis, Barboun et al. used inelastic neutron scattering (INS)

Received: June 10, 2022
Revised: July 19, 2022
Accepted: July 25, 2022
Published: August 5, 2022

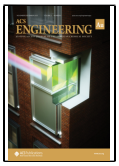

combined with sequential plasma and thermal treatments of N_2 and H_2 to identify NH_X species formed on Ni/γ-Al_2O_3 under plasma exposure, which were not observed when solely thermal treatments were applied.[39] Alternatively, Gibson et al. probed the local temperature, oxidation state, and overall structure of Pd nanoparticles for methane oxidation with *in situ* X-ray absorption spectroscopy under plasma stimulation.[40] While these studies represent significant contributions toward understanding specific plasma-catalyst systems, the techniques employed require specialized synchrotron radiation facilities, which can impede research advancement due to limited access to instrumentation for data collection.

Other approaches to observe the plasma-catalyst interface have exploited the ubiquity and versatility of Fourier transform infrared (FTIR) spectroscopy to detect functional groups on a solid surface. Stere et al. combined a He plasma jet with a modified diffuse reflectance (DRIFTS) cell to successfully identify isocyanate as the reactive surface intermediate in the low-temperature, Ag-catalyzed selective catalytic reduction of NO_x.[41] Other *in situ/operando* plasma studies have also used DRIFTS cells,[42,43] including a design[44] for a small-scale, helical surface discharge (HSD) developed by Turan et al. for millimeter-scale applications. While the HSD design and others based on DRIFTS are relatively simple to use and require minimal construction/modification, the cost of a new DRIFTS cell coupled with permanently modifying it may suppress interest and prevent widespread adoption. Additionally, from our experience with the HSD design, HSD plasma ignition can alter the sample packing through ejection of powder from the sample cup causing difficulties when correctly subtracting the background spectrum from the collected data. More sophisticated FTIR spectroscopy techniques have also been used, such as polarization-modulation infrared reflection-absorption spectroscopy (PM-IRAS), which uses both p- and s-polarized light to continually discriminate between gas-phase signals and surface-bound signals. Recently, an Ar-plasma jet and an optical emission spectroscopy (OES) probe were incorporated in a PM-IRAS cell to successfully observe surface-, gas-, and plasma-phase species simultaneously for the NTP-activated, non-oxidative coupling of methane on a model surface.[45]

While the infrared-based designs mentioned above have been largely successful at generating useful information about the plasma-surface interface, the sample configuration and metal housing of DRIFTS and PM-IRAS cells present additional engineering challenges when combining the high-voltage discharge with a partially exposed sample. These challenges have previously been addressed by generating a plasma jet in an inert gas with a low breakdown voltage (e.g., He or Ar) and then bringing the plume close enough to interact with the sample.[41,45] While this approach does expose the sample to a plasma, it is unclear how the plasma characteristics change relative to a discharge generated directly in the reactive gas.[46] Unlike DRIFTS and PM-IRAS, transmission IR requires the sample to be suspended directly in the path of the IR light source, which passes through the sample to the detector. This configuration allows electrodes to be placed on either side of the sample, generating a plasma discharge directly in the reactive gas encompassing the surface of interest. Several designs modifying traditional transmission cells have been implemented in recent years,[47−52] including a glow-discharge cell designed by Rivallan et al.,[53] which has already been used in several studies on NTP-activated CO_2 hydrogenation at pressures around 10^{-3} atm.[54−56] However, molecular gases have higher breakdown voltages and thus require designs that either (1) increase the applied voltage, (2) decrease the electrode gap, or (3) apply vacuum pressure to achieve a stable discharge according to Paschen's Law.[57] Because lab-scale modules are limited by how much voltage can safely be applied, a balance must be established between (2) and (3): reducing the electrode gap will restrict spectroscopic access to the sample while decreasing pressure causes the *in situ* conditions to deviate from real atmospheric-pressure plasma reactors, resulting in the "pressure gap" problem commonly faced in catalysis research.[58]

Here, we present an alternative, facile design for a plasma-transmission IR cell capable of surface-sensitive, *in situ/operando* measurements under a wide range of plasma conditions. The design and function of the cell are comparable to commonly used dielectric barrier discharge (DBD) plasma-catalytic reactors, and its inexpensive construction, quick sample preparation, and ability to simultaneously interface with commonplace analytical techniques such as FTIR, OES, and mass spectrometry (MS) promote its adoption as a widespread tool for rapidly obtaining large volumes of *in situ* plasma-catalysis data. The effectiveness of the cell was demonstrated using (1) plasma-assisted oxidation of 3-aminopropyl SBA-15 (AP-SiO_2) to establish plasma-surface contact and (2) low-temperature plasma-assisted nitrogen oxidation over a Pt/SiO_2 catalyst to provide an example of plasma−catalyst interactions.

2. EXPERIMENTAL SECTION

2.1. Design Overview

The design of the transmission plasma-IR cell was initially inspired by the transmission cell constructed and reported by Cybulskis et al.[59] Therefore, it can serve both plasma and thermal purposes once constructed (Figure 1). Additionally, the overall form of the plasma

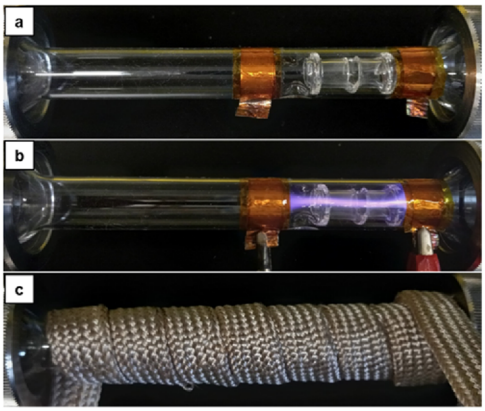

Figure 1. Plasma transmission cell (a) during plasma operation (b) and during thermal operation (c).

generation component can be easily adapted to other similar transmission cell designs that incorporate long quartz tubes to house the sample. Key adaptations to the original design are discussed, including (1) the addition of adjustable, non-invasive copper electrodes with an off-center sample placement, (2) the tapered cell diameter, (3) the temperature control system, and (4) the implementation of an OES probe.

2.2. Dimensions

A detailed schematic of the cell and sample holder with dimensional labels is provided in Figure 2. The cell is a fused quartz tube of length 157.2 mm with a tapered center (14.0 mm OD; 12 mm ID) and two

https://doi.org/10.1021/acsengineeringau.2c00026
ACS Eng. Au 2022, 2, 535−546

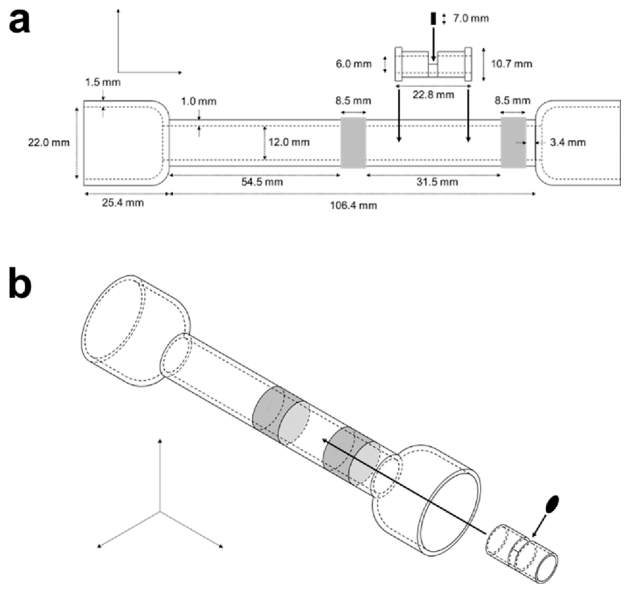

Figure 2. Orthographic (a) and isometric (b) views of the tube and sample holder (not to scale). Outside edges are solid lines, and inside edges are dashed lines. The copper electrodes are shaded light gray, the sample wafer is shaded black, and the quartz body is left unshaded.

electrodes positioned coaxially outside the tube. The cell is sealed by fittings identical to those used by Cybulskis et al. The tube length is specific to the sample compartment of a Bruker Vertex 70 FTIR spectrometer equipped with a liquid nitrogen-cooled mercury-cadmium-telluride (MCT) detector. The materials of construction for the sample holder are similar (fused quartz tube; 10.7 mm OD, 6.0 mm ID) with a recessed slit to hold a 7.0 mm diameter sample wafer. The sample can be heated *in situ* by heating tape tightly wrapped in a spiral around the full length of the cell (Figure 1). The electrodes are made from 8.5 mm wide copper tape with an electrically conductive adhesive (Kraftex) and wrapped ~1.1−1.5 times around the outer diameter with leading edge positions at 28.8 and 68.8 mm from the inlet of the tube. The electrodes are covered by insulating Kapton tape (Equity Baymers) to prevent unwanted discharging outside the cell. Additionally, all nearby metals are adequately grounded to ensure that a hazardous buildup of charge does not occur. The vacuum system features a needle valve placed downstream of the cell to control the applied pressure from an in-line vacuum pump (Welch Vacuum 2014B-01), allowing the operator to adjust the absolute pressure between 0.1 and 1.0 atm. The cell is suspended within the sample compartment of the spectrometer by two metal supports placed on either end of the tube. Each support is capable of elongating via an adjustable screw to position the sample wafer at the correct height within the incident beam.

2.3. Configuration

This unique electrode geometry was inspired by the design first reported by Teschke et al. for generating plasma jets,[60] and its non-invasive arrangement eliminates concern of possible catalytic activity originating from the electrode material. Additionally, the impermanence and adjustability of the electrodes provide significant freedom when choosing where to generate a NTP within the cell (e.g., post-plasma catalysis versus in-plasma catalysis studies). We found that the maximum achievable power and the absence of unwanted discharging to the metal fittings on the ends of the cell occurs with the high-voltage electrode at the center of the cell with the ground electrode near the inlet. This arranges the high voltage electrode equidistant from the grounded metal fittings and ensures the ground electrode offers the path of least resistance for plasma generation. To prevent the sample holder from moving axially along the cell during setup, optional indentations located 66 mm from the inlet of the tube were added to serve as backstops (omitted from Figure 2 for clarity). This location was chosen specifically so that the sample holder can either be centered between the electrodes (depicted in Figures 1 and 2) or at the midpoint of the cell. Additionally, the diameter of the cell was decreased by 44% compared to the Cybulskis et al. design[59] to facilitate gas breakdown at vacuum pressures closer to atmospheric by reducing the effective discharge gap, d_{eff} (eq 1). This increases the maximum operating pressure capable of achieving a stable discharge at the same breakdown voltage in the collision dominated regime of Paschen's Law.[57]

$$d_{\text{eff}} = \sqrt{\frac{(r^2 + d^2)^{3/2}}{d}} \tag{1}$$

Here, r is the radius of the ring electrodes and d is the linear distance between electrodes. Equation 1 shows that the effective discharge gap, d_{eff}, scales with $r^{3/2}$ and d, indicating that the radius of the ring electrode, r, has a more significant contribution toward decreasing the effective discharge gap and increasing the maximum operating pressure compared to the actual gap distance, d, between the electrodes. The smaller diameter tube was also chosen to fit a smaller sample wafer to minimize potential temperature and concentration gradients within the sample. As noted by Cybulskis et al., studies seeking quantitative determination of reaction rates and kinetic parameters can estimate the influence of potential temperature and concentration gradients for a specific reaction using Mears' criteria.[59,61] Additionally, the compact size of the Specac Mini Pellet Press used in this study combined with shut-off valves on both ends of the transmission cell allow each to be easily moved into and out of a N_2 atmospheric glovebox for preparation of highly air-sensitive samples.

2.4. Heating System

In our experience, internal temperature control poses a significant engineering challenge in both *in situ* spectroscopic systems and plasma-based systems. For most *in situ* spectroscopic systems, the limited space available in the instrument sample compartment prohibits the use of full-size tube furnaces that are commonly used in lab-scale reactors to control the temperature. The parent design overcame this issue by controlling the temperature of a bore-through brass block, which was able to rapidly heat and cool the sample thanks to a feedback temperature controller combined with the high thermal conductivity of brass.[59] However, we have found that for both this plasma system and others, the high voltage electrode tends to discharge to metal heating elements and thermocouples placed near the plasma zone, making it difficult to measure the bulk gas temperature and preventing feedback temperature controllers from being used. Additionally, the chosen heating element should be easily obtainable for any researcher and quickly removeable/replaceable between thermal and plasma treatments to conduct sequential studies similar to those performed by AlQahtani et al.[24] and the INS studies mentioned previously.[39] The solution chosen involves the use of standard heating tape commonly found in any laboratory setting wrapped in a co-axial spiral configuration around the quartz tube (Figure 1). The bulk gas temperature near the sample wafer is then calibrated with a thermocouple against the output of a variable transformer (Variac) that controls the input power to the heating tape. Two different heating tape models were used: model A (BriskHeat BIH051020: 105 W, 0.5″ width × 24″ length) and model B (BriskHeat FGH051-040 L: 210 W, 0.5″ width × 48″ length). To prolong the lifetimes of both heating tape models, model A is predominantly used for thermal applications requiring higher temperatures up to 400 °C, where model B is only used for applications below 300 °C. If additional temperature control during thermal operation is desired (e.g., for heating at a controlled ramp rate), thermocouples can be inserted into the sample volume to allow operation with feedback control systems.

2.5. Integration with OES and MS

The transmission cell can be easily integrated with additional probes to analyze the plasma phase and effluent gases exiting the reactor

https://doi.org/10.1021/acsengineeringau.2c00026
ACS Eng. Au 2022, 2, 535−546

zone. In this study, an OES probe (Ocean Optics USB2000 + XR1 spectrometer with THORLABS F280SMA-A collimator and Ocean Insight QP300−1-SR fiber optic cable) was positioned external to the transparent quartz cell body via a ring stand clamp to observe the photons emitted from plasma-stimulated species within the cell. Additionally, a Pfeiffer OmniStar process MS (200 amu) was affixed to the effluent side of the reaction chamber to analyze the production and evolution of stable, gas-phase products.

2.6. AP-SiO_2 Synthesis

SBA-15 was synthesized according to previous reports.[62] SBA-15 was dried under vacuum at 200 °C and stored in a N_2 drybox. The SBA-15 was post-synthetically modified with primary amine functionalities through reaction with 3-aminopropyltrimethoxylsilane (Sigma-Aldrich 97%).[63] In a typical procedure, 2.0 g of 3-aminopropyltrimethoxysilane was added to 2 g of SBA-15 dispersed in dry toluene (~50 mL). The mixture was then stirred in a nitrogen atmosphere for 24 h at room temperature to homogenize the aminopropyl functionalization on the silica surface. A white solid was filtered from the mixture, washed with dry toluene, dried under vacuum at 70 °C for 3 h, and stored in the N_2 drybox. The amine loading of the resulting AP-SiO_2 sample was determined as 1.9 mmol/g by thermogravimetric analysis of a temperature programmed oxidation.

2.7. Pt/SiO_2 Catalyst Synthesis

The 5 wt % Pt/SiO_2 catalyst was synthesized onto a fumed silica support (Spectrum Chemical: Aerosil 200, 175−225 m^2/g) by an incipient wetness impregnation procedure. The fumed silica (2.00 g) was first dried and calcined at 200 °C for 12 h. Next, 0.30 g of dihydrogen hexachloroplatinate(IV) hexahydrate (Beantown Chemical, 99.95%) was dissolved in 2.52 g of deionized water and added dropwise to the fumed silica while stirring. The material was dried at 120 °C for 12 h and reduced in pure hydrogen at 200 °C for 5 h (ramped at 1 °C/min). The site density of the Pt/SiO_2 was 44.1 μmol/g measured by CO pulse chemisorption. The surface areas of the fumed silica support (206.8 m^2/g) and the Pt/SiO_2 (194.6 m^2/g) were measured by N_2 physisorption analysis at 77 K (Quantichrome NOVA 2200e).

2.8. Procedures for Application 1: Plasma Oxidation of Primary Amine-Functionalized SBA-15

The AP-SiO_2 sample was first prepared into a self-supporting wafer using a hydraulic pellet press (Specac Mini Pellet Press). The 7 mm diameter wafer was pressed with 1.0 ton of force for 5 min. The sample was subsequently weighed and placed into the sample holder inside the transmission cell. The system was checked for leaks prior to operation. The sample was then pretreated at 120 °C for 1.5 h under 100 mL/min of 0.1 atm pure He flow (Airgas 99.997% purity). Pretreatment at 120 °C was chosen based on CO_2 desorption experiments performed on similar materials.[63] For the thermal only experiment, a background spectrum was taken under the pretreatment conditions at the end of 1.5 h. The gas feed was then adjusted to 100 mL/min of 1% O_2/He (Airgas mixed tank, 0.9999 mol % O_2, balance He) with all other conditions maintained. Scans were taken every 5 min. For the plasma experiment, the sample was cooled after pretreatment to room temperature under 100 mL/min of 0.1 atm pure He. The plasma was then switched on under the same He flow and adjusted to the desired setting. A 2 W plasma was used, which corresponds to a specific energy input (SEI) of 1200 J/L. Here, SEI is defined as the plasma power divided by the total gas flow rate. The plasma was kept relatively low to minimize the resistive heating (outer surface temperature was maintained at 60 °C and recorded by thermal imaging camera: RIGID tools, model RT-9x) and to ensure the bulk gas temperature remained well below 120 °C. Because the background spectrum is dependent on the temperature, the plasma was allowed to reach its autogenous temperature under the inert gas flow for 10−15 min before the background spectrum was recorded. Then, the gas feed was adjusted to 100 mL/min of 1% O_2/He with all other conditions maintained. The plasma power was measured by integration of charge-voltage plots,[64] and IR scans were recorded every 5 min.

2.9. Procedures for Application 2: Catalytic Low-Temperature Nitrogen Oxidation

The Pt/SiO_2 and SiO_2 samples were first prepared into 7 mm-diameter self-supporting wafers using the same hydraulic press (Specac Mini Pellet Press). Both samples were undiluted and pressed with 1.75 tons of force for 5 min. The sample wafers were then weighed and loaded into the cell, and the system was checked for leaks. Both Pt/SiO_2 and SiO_2 were pretreated at 300 °C for at least 1 h under 30 mL/min of 0.3 atm pure H_2 flow (Airgas 99.999% purity). The higher pretreat pressure was chosen to increase the gas collisions with the surface and shorten the time required for pretreatment. For the thermal only experiment, the Pt/SiO_2 pellet was allowed to cool after pretreatment to 150 °C under 0.1 atm of 100 mL/min He and 30 mL/min N_2 (Airgas 99.999% purity) flow, and a background spectrum was recorded. The gas feed was then switched to 100 mL/min of 1% O_2/He and 30 mL/min N_2 with all other conditions maintained. IR scans were recorded every 5 min.

For the plasma experiments, the sample wafer was allowed to cool to room temperature under 0.1 atm of 100 mL/min He and 30 mL/min N_2 flow. The plasma was then switched on under the same He/N_2 flow and adjusted to the desired setting. A 0.3 W plasma was used, which corresponds to an SEI of 138 J/L. The sample was allowed to reach autogenous temperature for 10−15 min before a background spectrum was recorded. The gas feed was then switched to 100 mL/min of 1% O_2/He and 30 mL/min N_2 with all other conditions maintained. The plasma power was subsequently measured by integration of charge-voltage plots,[64] and IR scans were recorded every 5 min.

3. RESULTS AND DISCUSSION

3.1. Thermal Control Validation

Before the *in situ*/*operando* experiments were conducted, we first sought to statistically quantify the accuracy and reproducibility of the heating system in the plasma cell for gases of varying thermal conductivity (He and N_2) at both high (0.3 atm) and low (0.1 atm) pressures. The internal temperature was measured by a thermocouple placed near the sample holder, and the heating tape was removed and replaced after each trial for a total of three trials per data set. The calibrations given in Figure 3 show temperature control to

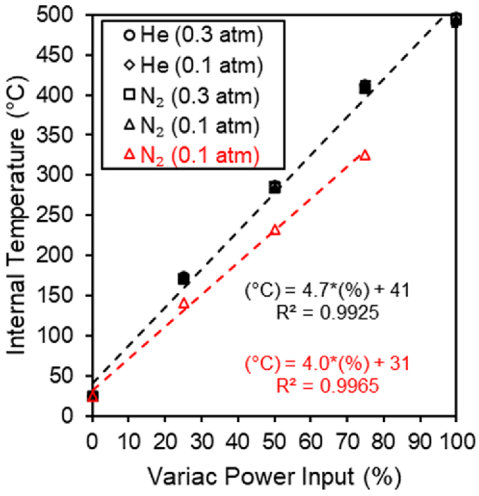

Figure 3. Variac temperature calibration for use with heating tape models A (black) and B (red). Total flowrate is 100 mL/min. Temperature is measured by an internally placed thermocouple. Heating tape was removed and replaced after each trial. Error bars on model A represent one standard deviation after three trials per data set.

https://doi.org/10.1021/acsengineeringau.2c00026
ACS Eng. Au 2022, 2, 535−546

within ±10 °C with 95% confidence. The calibrations also show that temperature control is insensitive to both the thermal conductivity of the gas and the absolute pressure over the normal operating range of the system (0.1−0.3 atm).

For temperature comparisons between thermal and plasma experiments, an estimation of the autogenous temperature of the plasma is also required. We varied both the pressure and applied power of a pure N_2 discharge over the full operating range of the cell and measured the resulting maximum surface temperature (located on the surface of the high voltage electrode) with a thermal imaging camera. The results are given in Figure 4, which serves to both estimate the resistive heating of the plasma and show how the pressure can be adjusted to shift the range of accessible plasma powers.

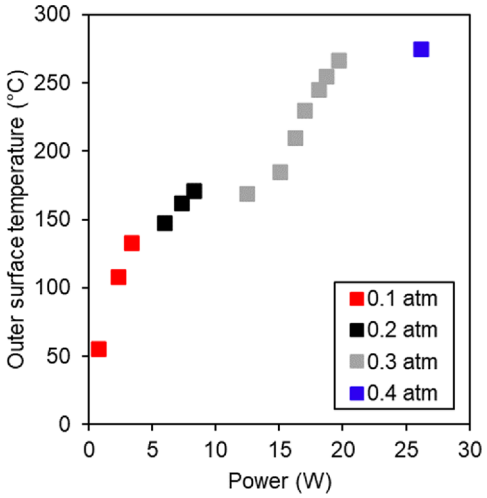

Figure 4. Resistive heating as a function of plasma power and overall pressure. The plasma was generated at a constant frequency (23.5 kHz) with an empty sample holder and 100 mL/min pure N_2 flow.

3.2. Application 1: Plasma Oxidation of Primary Amine-Functionalized SBA-15

The primary function of the transmission plasma-IR cell is the observation of plasma interactions with different types of solid materials. Therefore, we begin by providing evidence that the system can both induce and detect surface changes in response to plasma stimulation. To demonstrate this ability, plasma-induced oxidation of an organic/inorganic hybrid aminosilica material (AP-SiO_2) was conducted. The AP-SiO_2 (Scheme 1) used here is part of a widely studied class of functionalized materials with applications in CO_2 capture and heterogeneous catalysis.[63,65−69] This class of materials was chosen for several reasons, including (1) the distinct IR features of the organic functionality and oxidation products (e.g., NO_X), (2) their straightforward synthesis onto silica supports, (3) the high achievable loading of the 3-aminopropyl groups onto the SBA-15, and (4) the existing literature characterizing the behavior and stability of primary amines in oxygen environments. For example, several previous works have reported that primary amines will oxidize at low temperatures in the presence of reactive oxygen derivatives such as ozone (O_3).[70−73] This process was shown to selectively form nitroalkanes in high yields without oxidizing the carbon framework. Therefore, we hypothesized the oxygen plasma would similarly generate nitroalkane derivatives from the primary amines on AP-SiO_2.

Scheme 1. Chemical Structure of Unreacted AP-SiO_2

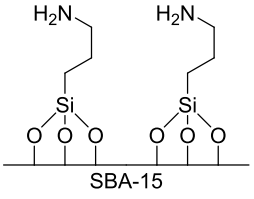

Bollini et al. demonstrated using solid-state ^{13}C nuclear magnetic resonance spectroscopy that 3-aminopropyl groups on silica remain unchanged in pure O_2 up to at least 135 °C.[74] We used this finding as a thermal benchmark for comparison to plasma stimulation experiments. To verify this outcome in our own system, we conducted thermal control experiments with 100 mL/min of 1% O_2/He at 120 °C and 200 °C and obtained the same result. The data at 120 °C are provided in Figure 5a (black solid curve), which indeed shows no spectral changes were observed after 30 min of thermal oxygen treatment.

Next, an equivalent experiment was performed with plasma stimulation of the 100 mL/min of 1% O_2/He feed at 60 °C autogenous temperature. The background-subtracted spectra of the AP-SiO_2 surface after 30 min are shown in Figure 5a. Several changes were observed at the higher frequencies of the fingerprint region (1600−1300 cm^{-1}), indicating plasma-surface reactions are taking place that were not observed thermally. The absence of negative peaks in the C−H stretching region (2850−3000 cm^{-1}) suggests that the propyl backbones of the amino groups are not oxidized by the plasma and remain intact (inset of Figure 5a). This observation is supported by the MS trace for CO_2 (44 m/z) given in Figure 5b, which shows that no CO_2 was formed upon introducing O_2 (32 m/z) to the system. Additionally, no evidence for either NO (30 m/z) or NO_2 (46 m/z) was present from these experiments, further suggesting that the nitrogen remains tethered to the surface by the propyl backbone.

In Figure 5a, the negative peak in the N-H bending range (1590−1627 cm^{-1}) represents the disappearance of amino groups upon reaction with an oxygen plasma.[75] This combined with the generation of H_2O (18 m/z) shown in Figure 5b indicates oxidation of the surface amines. The likely products of this oxidation are R-NO_2 species,[70−73] which are expected to have strong IR signals in the 1650−1300 cm^{-1} region.[76] Looking at the FTIR spectra in Figure 5a, the sharp peaks at 1556 and 1381 cm^{-1} are characteristic of the symmetric and asymmetric stretching of nitro (-NO_2) groups, respectively.[76] This result is in agreement with previous works that show high yields of nitroalkanes from reacting primary amines with ozone.[70−73] The other prominent peak at 1435 cm^{-1} (Figure 5a) is associated with the C−H bending in the alkyl backbone,[77] which is observed in both nitroalkanes and amines.[78] The increase in the intensity of the 1435 cm^{-1} band with time is related to changes in the local chemical environment surrounding the alkyl backbone rather than the formation of C-H bonds.[79] Other smaller peaks are observed in Figure 5a, including carbonyl and imine stretches between 1650 and 1750 cm^{-1}.[80,81] However, the extinction coefficients for these species are relatively large,[80,81] indicating low surface concentration. The other peaks in this region likely arise from trapped water vapor, which has many strong rovibrational peaks in this region.[82]

https://doi.org/10.1021/acsengineeringau.2c00026
ACS Eng. Au 2022, 2, 535−546

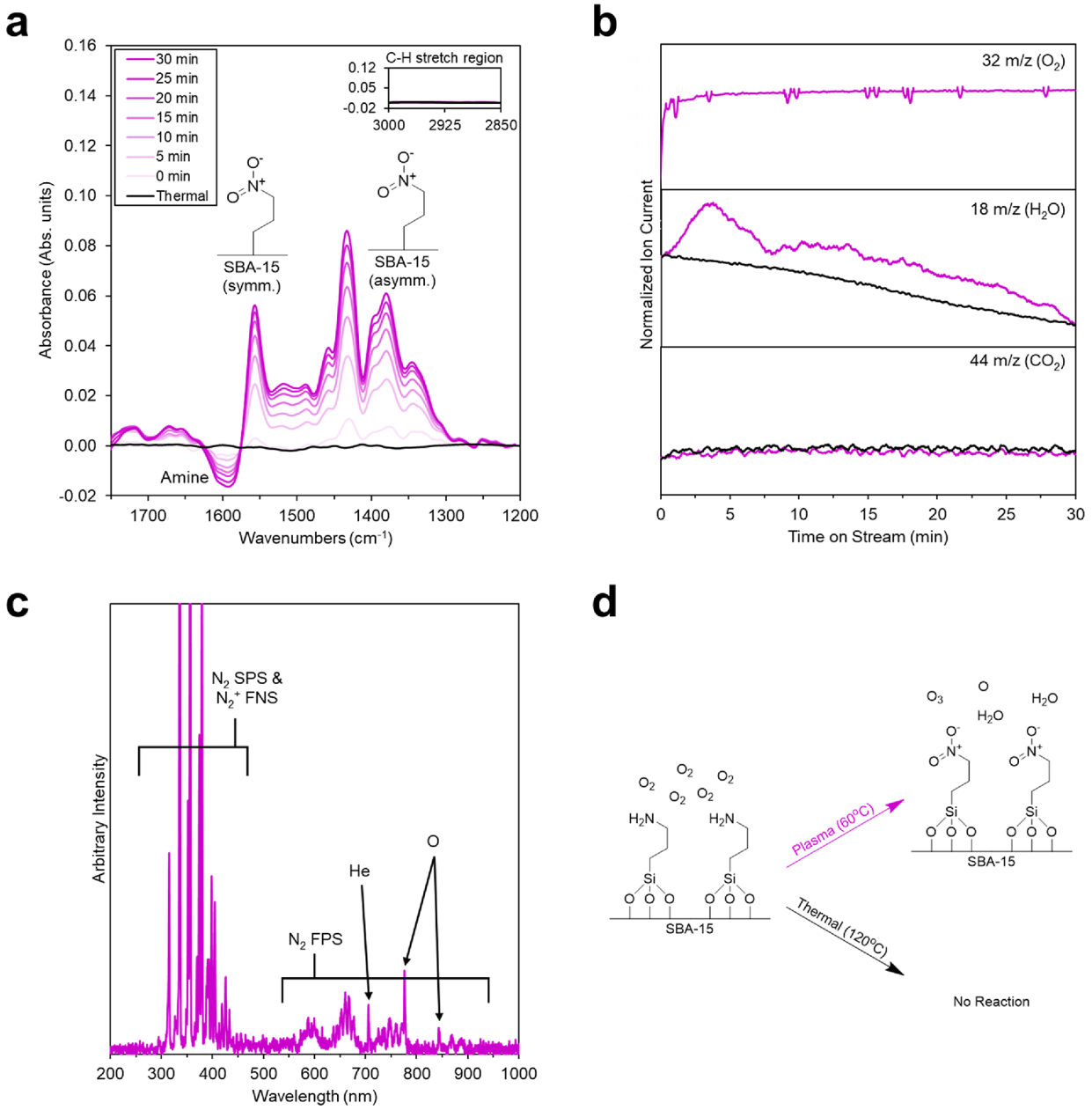

Figure 5. FTIR (a), MS (b), and OES (c) data with observed surface species (d) from plasma (2 W; 60 °C; 8.6 mg; purple) and thermal (120 °C; 4.3 mg; black) oxidation of AP-SiO_2 in a 100 mL/min of 1% O_2/He feed at 0.1 atm. FTIR spectra are baseline corrected and background subtracted. OES spectrum is background subtracted to correct for stray light.

The plasma phase was characterized using OES, which detects photons emitted by various electronic relaxations of both atomic and molecular species. Figure 5c shows a representative OES spectrum of the 1% O_2/He plasma taken after 15 min. The spectrum has the He I feature at 706 nm ($3^3S \rightarrow 2^3P$) as well as clear triplet O I features at 777 nm ($3^5P \rightarrow 3^5S$) and 845 nm ($3^3P \rightarrow 3^3S$).[83] The presence of electronically excited atomic oxygen is evidence that the dioxygen in the feed is dissociated by the plasma, resulting in the formation of O_3.[84] Due to the half-life of O_3 (10^3 s) compared to the half-life of atomic oxygen (10^{-6} s), O_3 is likely interacting with internal amines by diffusing within the pores of the SBA-15, whereas atomic oxygen can only interact with the species outside the pores.[84] Additionally, the OES spectrum shows strong features associated with the $N_2(B^3\Pi_g \rightarrow A^3\Sigma_u^+)$ first positive system (FPS), $N_2(C^3\Pi_u \rightarrow B^3\Pi_g)$ second positive system (SPS), and $N_2^+(B^2\Sigma_u^+ \rightarrow X^2\Sigma_g^+)$ first negative system (FNS),[83,85] which are presumed to be from air contamination. Spectral lines due to foreign gases are commonly seen in OES for even the purest He feed streams due to the ability of excited He atoms to efficiently ionize impurities through Penning ionization, causing the impurities to have disproportionately intense OES signals.[83,85] Additionally, the MS trace detected no nitrogen oxidation products when oxygen was introduced, and the vacuum system was checked for leaks before each experiment. Therefore, the concentration of air in the system is considered negligible. While any degree of contamination is generally undesirable, the N_2 rovibrational bands can be used to quickly estimate the rotational temperature of N_2 as a proxy for the bulk gas

https://doi.org/10.1021/acsengineeringau.2c00026
ACS Eng. Au 2022, 2, 535−546

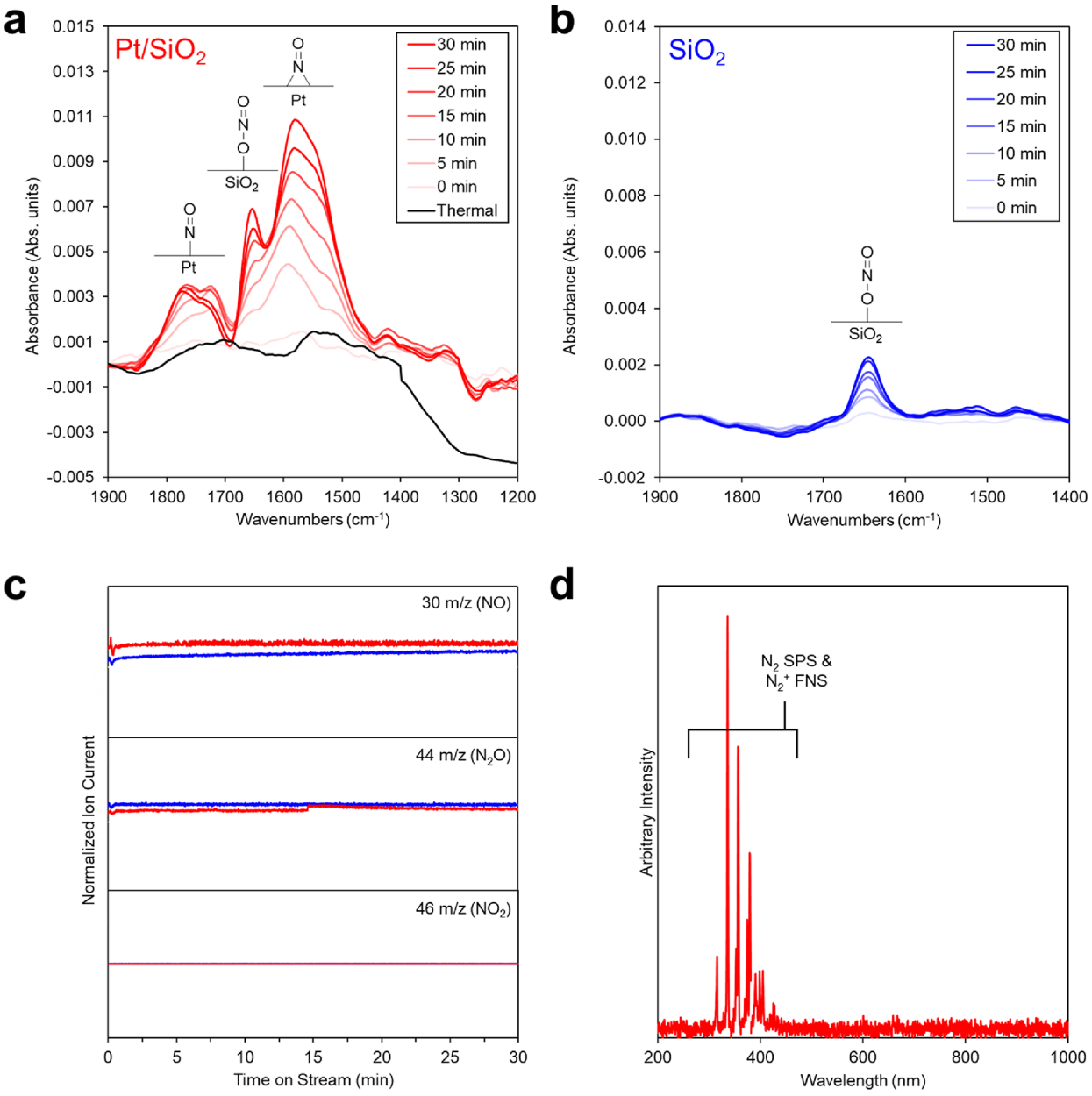

Figure 6. FTIR (a,b), MS (c), and OES (d) data of 0.3−0.4 W plasma oxidation of N_2 with Pt/SiO_2 (red; 4.6 mg pellet) and SiO_2 (blue; 2.1 mg pellet) in a 30 mL/min N_2, 1 mL/min O_2, and 99 mL/min He feed at 0.1 atm. Thermal treatment (black) of Pt/SiO_2 was at 150 °C. Plasma autogenous temperature was 39 °C. FTIR spectra are baseline corrected and background subtracted. OES spectrum is background subtracted to correct for stray light.

temperature.[85,86] Unfortunately, this technique requires a spectral resolution of at least 0.2 nm, which is outside the capability of the spectrometer used here (~2 nm resolution).[86] Nevertheless, additional opportunities exist to couple this system with more specialized OES techniques that further characterize the plasma by calculating the electronic/vibrational temperature, the electron density, the degree of ionization, and the species mole fractions.

The FTIR, MS, and OES results clearly suggest that oxygen plasma selectively oxidized primary amines to nitro groups without altering the hydrocarbon tether (Figure 5d). The use of NTP to perform this transformation obviates the need for harmful reactants that would typically be used (e.g., hypofluorous acid, Caro's acid, and organic peroxides), and the resulting nitro groups can be readily converted to other desired functional groups.[73] This has clear applications in the synthesis of biomaterials, where surface hydrophobicity needs to be carefully controlled to either prevent or promote the adhesion of cells and the growth of biofilms.[87] The plasma transmission cell was capable of monitoring the evolution of surface-bound species over time, demonstrating its usefulness as an *in situ* characterization technique.

3.3. Application 2: Catalytic Low-Temperature Nitrogen Oxidation

After establishing the capability of the transmission plasma-IR setup to directly observe plasma-surface interactions of organic/inorganic materials, we further demonstrate the application of this system to observing adsorbates on metal surfaces during plasma-assisted nitrogen oxidation. Rather than attempting to determine plasma-catalyst interactions as has

https://doi.org/10.1021/acsengineeringau.2c00026
ACS Eng. Au 2022, 2, 535−546

been done previously,[88] these experiments are aimed at characterizing the catalyst surface *in situ* under realistic conditions.

Plasma technologies for chemical synthesis date back to the early 1900s when the Birkeland−Eyde process for nitric acid synthesis became the first ever plasma system to be commercially implemented.[89] A thermal, high temperature, equilibrium plasma reactor was used to produce nitric oxide (NO) by activating nitrogen and oxygen in the ambient air and absorbing the effluent stream in water to form nitric acid.[89] However, the process was ultimately abandoned by industry due to poor energy efficiency and low conversion.[89] More recently, there has been renewed interest in plasma-activated nitrogen activation, especially in combination with a catalyst to reduce the energy barrier for nitrogen dissociation.[18,33−39,52,88] The nitrogen oxidation reaction is an ideal candidate to be studied by this design primarily because its large endotherm ($N_2 + O_2 \rightarrow 2NO$; $\Delta H = 90$ kJ/mol[90]) makes it severely thermodynamically limited. Thus, its light-off temperature is beyond the capability of standard thermal IR cells (equilibrium concentration of NO in synthetic air is 100 ppm at 1000 K[89]), requiring a non-thermal plasma to achieve high enough conversions to study the reaction *in situ*. Additionally, the products (NO_X) are highly IR-active, whereas the reactants (N_2 and O_2) are IR-inactive, which ensures that any IR signal observed is exclusively from the products.

To demonstrate the lack of thermal reactivity between N_2 and O_2, we performed a thermal control experiment on Pt/SiO_2 at 150 °C with 30 mL/min of N_2 and 100 mL/min of 1% O_2/He. As expected, the IR spectrum showed no detectable changes at the catalyst surface after 30 min of thermal exposure (Figure 6a). This result also eliminates concern that observed peaks in subsequent experiments are due to impurities from the gas tanks adsorbing onto the surface.

Next, a second control experiment was performed under the same conditions on SiO_2 under a 0.3 W plasma treatment and 39 °C autogenous temperature. The FTIR results given in Figure 6b show a single peak in the N−O stretching region at 1648 cm^{-1}, which was assigned to nitrite species[81] covalently bound to silicon as Si−O−N═O.[90] Although covalently bonded silicon nitrite is generally not observed in thermal NO_X-adsorption studies on silica materials,[91] Chao and Lunsford first reported its presence after NO adsorption on decationated zeolite Y up to 200 °C.[90] They compared the results of several Y-type zeolites and only observed the silicon nitrite on the decationated Y, which contains oxygen vacancies as trigonal Si^+ centers.[92] This led to the conclusion that the Si^+ oxygen vacancy was a required precursor to the formation of silicon nitrite species.[90] Because NTP is known to induce oxygen vacancy defects in silica,[93−95] we can conclude from the IR data in Figure 6b that the plasma generated by the transmission cell is creating trigonal Si^+ centers, which interact with NO produced in the plasma phase to form silicon nitrite groups.

The FTIR results for Pt/SiO_2 under the same plasma conditions as the SiO_2 control experiment are given in Figure 6a. The IR spectra have three main features at 1700-1800, 1653, and 1580 cm^{-1}, with the middle peak being previously assigned to silicon nitrite.[90] All peaks remained unchanged after the plasma was turned off and the cell was purged with He. Based on other literature reports, the features at 1700−1800 and 1580 cm^{-1} are linear and bent NO species adsorbed on Pt, respectively.[96,97] The linear region is further divided into two distinct peaks around 1770 and 1720 cm^{-1}, which correspond to linearly bound NO on different Pt sites. From literature FTIR studies on single crystal Pt surfaces, we can assign the 1770 cm^{-1} peak to the Pt(110) surface and the 1720 cm^{-1} peak to the Pt(111) surface; no linearly bound NO is expected on Pt(100).[97−100] These reports also suggest that the 1580 cm^{-1} peak assigned to bent NO is broad enough to account for adsorption on all three low-index planes of Pt. As time-on-stream increases, Figure 6a shows (1) the 1770 cm^{-1} peak intensity increases until reaching a steady state after 15 min, (2) the 1720 cm^{-1} peak intensity reaches a maximum after 15 min and begins decreasing, and (3) the 1580 cm^{-1} peak intensity steadily increases over the full 30 min. Therefore, the coverages of the corresponding species follow the same progression with time.

The MS traces of the expected nitrogen oxide products (NO 30 m/z, N_2O 44 m/z, and NO_2 46 m/z) for both the SiO_2 and Pt/SiO_2 are given in Figure 6c. The production rates of all three products were below the detection limits for the MS used here, and no clear improvement of Pt/SiO_2 over SiO_2 was observed. This is not unexpected considering Ma et al. has shown that for O_2/N_2 molar ratios above 0.01 (here we use 0.03), the oxygen species dominate the Pt sites and slow the production of NO to near plasma only background levels with negligible amounts of N_2O and NO_2 formed.[88] The lack of detectable products is also likely a consequence of the low SEI used here (138 J/L), which has been shown to scale linearly with reaction rates due to decreased generation of discharge filaments containing excited species.[33] This was supported by the OES spectrum given in Figure 6d, which is representative of the plasma under these conditions because no changes in the OES spectra were observed over time or between materials. Figure 6d shows only features associated with the SPS ($C^3\Pi_u \rightarrow B^3\Pi_g$) and FNS ($B^2\Sigma_u^+ \rightarrow X^2\Sigma_g^+$) of N_2, which was likely excited through Penning collisions with He.[83,85] Additionally, the absence of atomic O/N lines and NO systems suggests that these species are either absent altogether or only present in low concentrations. However, the IR data showing adsorption of nitrogen oxides on the surface of the Pt/SiO_2 catalyst suggests that atomic O/N and molecular NO_X are likely present in the plasma-phase.

The goal of this example application was to demonstrate the ability of the cell to collect information on the system under realistic reactor conditions. A lack of information from both OES and MS highlighted the importance of studying plasma-catalysis *in situ* and with multiple characterization techniques to obtain the full picture. Here, the IR data was key in drawing conclusions about the catalyst under plasma exposure, giving merit to the design and demonstrating its functionality for gathering information about the plasma-catalyst interface.

CONCLUSIONS

This work presents a simple design for a plasma-capable IR transmission cell for probing a surface under plasma stimulation. The materials for constructing the IR cell are ubiquitous and inexpensive, ensuring that the technology is available to any researcher studying plasma-surface coupling. Additionally, the design is easily customizable to suit specific needs (e.g., use of vacuum manifold for controlled dosing,[59] in-plasma vs post-plasma configurations,[2] integration with step-scan technique for microsecond resolution,[53,55] etc.) and can be paired with additional analytical and/or characterization techniques such as MS and OES. The thermal control of the

https://doi.org/10.1021/acsengineeringau.2c00026
ACS Eng. Au 2022, 2, 535−546

cell was tested at different pressures (0.1 and 0.3 atm) and feed gases (He and N_2), and the setpoint temperature was found to be reproducible to ±10 °C with 95% confidence across all conditions.

To verify the ability to both promote and recognize plasma effects on a surface, the oxidation of primary amine-functionalized SBA-15 was performed as an example application of the cell. The combined results from FTIR, MS, and OES lead to the conclusion that plasma generated reactive oxygen derivatives selectively oxidized the primary amines to nitro groups without further oxidation of the hydrocarbon linker to the support. This result was supported by literature, showcasing the ability to generate reliable conclusions about plasma-surface interactions. As a second example application, the cell was used to observe surface species on a Pt/SiO_2 catalyst for plasma-assisted nitrogen oxidation. IR results from the support-only experiment identified silicon nitrates formed by reaction with NO_X and plasma-generated oxygen vacancies on the silica surface. On Pt/SiO_2, both linear and bent NO species adsorbed on several Pt facets, and the cell was able to track the waxing and waning of these species on the catalyst surface over time. These results highlight the utility of this plasma cell and establish its capacity to study plasma-catalysis *in situ*.

AUTHOR INFORMATION

Corresponding Author

Jason C. Hicks − *Department of Chemical and Biomolecular Engineering, University of Notre Dame, Notre Dame, Indiana 46556, United States;* orcid.org/0000-0002-5054-2874; Email: jhicks3@nd.edu

Author

Russell J. Clarke − *Department of Chemical and Biomolecular Engineering, University of Notre Dame, Notre Dame, Indiana 46556, United States*

Complete contact information is available at: https://pubs.acs.org/10.1021/acsengineeringau.2c00026

Notes

The authors declare no competing financial interest.

ACKNOWLEDGMENTS

Work performed by R.J.C. is supported by the Department of Energy under Award DE-SC0021107 and the Engineering Research Centers Program of the National Science Foundation under NSF Cooperative Agreement no. EEC1647722. Parts and equipment for the transmission cell were funded by the US Air Force Office of Scientific Research under Award No. FA9550-18-1-0157.

REFERENCES

(1) Go, D. B. Ionization and Ion Transport: A Primer for the Study of Non-Equilibrium, Low-Temperature Gas Discharges and Plasmas. In *Ionization and Ion Transport: A primer for the study of non-equilibrium, low-temperature gas discharges and plasmas*; IOP Publishing, 2018, DOI: 10.1088/978-1-6817-4601-2ch1.

(2) Bogaerts, A.; Tu, X.; Whitehead, J. C.; Centi, G.; Lefferts, L.; Guaitella, O.; Azzolina-Jury, F.; Kim, H. H.; Murphy, A. B.; Schneider, W. F.; Nozaki, T.; Hicks, J. C.; Rousseau, A.; Thevenet, F.; Khacef, A.; Carreon, M. The 2020 Plasma Catalysis Roadmap. *J. Phys. D: Appl. Phys.* **2020**, *53*, 443001.

(3) Neyts, E. C. Plasma-Surface Interactions in Plasma Catalysis. *Plasma Chem. Plasma Process.* **2016**, *36*, 185−212.

(4) Weltmann, K.-D.; von Woedtke, T. Plasma Medicine—Current State of Research and Medical Application. *Plasma Phys. Controlled Fusion* **2017**, *59*, No. 014031.

(5) Adamovich, I.; Baalrud, S. D.; Bogaerts, A.; Bruggeman, P. J.; Cappelli, M.; Colombo, V.; Czarnetzki, U.; Ebert, U.; Eden, J. G.; Favia, P.; Graves, D. B.; Hamaguchi, S.; Hieftje, G.; Hori, M.; Kaganovich, I. D.; Kortshagen, U.; Kushner, M. J.; Mason, N. J.; Mazouffre, S.; Thagard, S. M.; Metelmann, H.-R.; Mizuno, A.; Moreau, E.; Murphy, A. B.; Niemira, B. A.; Oehrlein, G. S.; Petrovic, Z. L.; Pitchford, L. C.; Pu, Y.-K.; Rauf, S.; Sakai, O.; Samukawa, S.; Starikovskaia, S.; Tennyson, J.; Terashima, K.; Turner, M. M.; van de Sanden, M. C. M.; Vardelle, A. T. 2017 Plasma Roadmap: Low Temperature Plasma Science and Technology. *J. Phys. D: Appl. Phys.* **2017**, *50*, 323001.

(6) Mai-Prochnow, A.; Murphy, A. B.; McLean, K. M.; Kong, M. G.; Ostrikov, K. K. Atmospheric Pressure Plasmas: Infection Control and Bacterial Responses. *Int. J. Antimicrob. Agents* **2014**, *43*, 508−517.

(7) Lin, A.; de Backer, J.; Quatannens, D.; Cuypers, B.; Verswyvel, H.; de La Hoz, E. C.; Ribbens, B.; Siozopoulou, V.; van Audenaerde, J.; Marcq, E.; Lardon, F.; Laukens, K.; Vanlanduit, S.; Smits, E.; Bogaerts, A. The Effect of Local non-thermal Plasma Therapy on the cancer-immunity Cycle in a Melanoma Mouse Model. *Bioeng. Transl. Med.* **2022**, *e10314*, 1−18.

(8) K. P. Veerapandian, S.; de Geyter, N.; Giraudon, J.-M.; Lamonier, J.-F.; Morent, R. The Use of Zeolites for VOCs Abatement by Combining Non-Thermal Plasma, Adsorption, and/or Catalysis: A Review. *Catalysts* **2019**, *9*, 98.

(9) van Durme, J.; Dewulf, J.; Leys, C.; van Langenhove, H. Combining Non-Thermal Plasma with Heterogeneous Catalysis in Waste Gas Treatment: A Review. *Appl. Catal., B* **2008**, *78*, 324−333.

(10) Lee, C. G. N.; Kanarik, K. J.; Gottscho, R. A. The Grand Challenges of Plasma Etching: A Manufacturing Perspective. *J. Phys. D: Appl. Phys.* **2014**, *47*, 273001.

(11) Oehrlein, G. S.; Metzler, D.; Li, C. Atomic Layer Etching at the Tipping Point: An Overview. *ECS J. Solid State Sci. Technol.* **2015**, *4*, N5041−N5053.

(12) Profijt, H. B.; Potts, S. E.; van de Sanden, M. C. M.; Kessels, W. M. M. Plasma-Assisted Atomic Layer Deposition: Basics, Opportunities, and Challenges. *J. Vac. Sci. Technol., A* **2011**, *29*, 050801.

(13) Ostrikov, K.; Murphy, A. B. Plasma-Aided Nanofabrication: Where Is the Cutting Edge? *J. Phys. D: Appl. Phys.* **2007**, *40*, 2223−2241.

(14) Mangolini, L.; Thimsen, E.; Kortshagen, U. High-Yield Plasma Synthesis of Luminescent Silicon Nanocrystals. *Nano Lett.* **2005**, *5*, 655−659.

(15) Schwan, J.; Wagner, B.; Kim, M.; Mangolini, L. Controlled Growth of Silicon Particles via Plasma Pulsing and Their Application as Battery Material. *J. Phys. D: Appl. Phys.* **2022**, *55*, No. 094002.

(16) Zhang, Z.; Wilson, J. L.; Kitt, B. R.; Flaherty, D. W. Effects of Oxygen Plasma Treatments on Surface Functional Groups and Shear Strength of Carbon Fiber Composites. *ACS Applied Polymer Materials* **2021**, *3*, 986−995.

(17) Neyts, E. C.; Ostrikov, K. K.; Sunkara, M. K.; Bogaerts, A. Plasma Catalysis: Synergistic Effects at the Nanoscale. *Chem. Rev.* **2015**, *115*, 13408−13446.

(18) Barboun, P. M.; Hicks, J. C. Unconventional Catalytic Approaches to Ammonia Synthesis. *Annu. Rev. Chem. Biomol. Eng.* **2020**, *11*, 503−521.

(19) Mehta, P.; Barboun, P.; Go, D. B.; Hicks, J. C.; Schneider, W. F. Catalysis Enabled by Plasma Activation of Strong Chemical Bonds: A Review. *ACS Energy Lett.* **2019**, *4*, 1115−1133.

(20) Whitehead, J. C. Plasma-Catalysis: The Known Knowns, the Known Unknowns and the Unknown Unknowns. *J. Phys. D: Appl. Phys.* **2016**, *49*, 243001.

(21) Bogaerts, A.; Neyts, E. C.; Guaitella, O.; Murphy, A. B. Foundations of Plasma Catalysis for Environmental Applications. *Plasma Sources Sci. Technol.* **2022**, *31*, No. 053002.

(22) Zhu, X.; Liu, J.; Hu, X.; Zhou, Z.; Li, X.; Wang, W.; Wu, R.; Tu, X. Plasma-Catalytic Synthesis of Ammonia over Ru-Based Catalysts: Insights into the Support Effect. *J. Energy Inst.* **2022**, *102*, 240−246.
(23) Tu, X.; Gallon, H. J.; Twigg, M. V.; Gorry, P. A.; Whitehead, J. C. Dry Reforming of Methane over a Ni/Al2O3 Catalyst in a Coaxial Dielectric Barrier Discharge Reactor. *J. Phys. D: Appl. Phys.* **2011**, *44*, 274007.
(24) AlQahtani, M. S.; Wang, X.; Knecht, S. D.; Bilén, S. G.; Song, C. Plasma-Enhanced Catalytic Reduction of SO2: Decoupling Plasma-Induced Surface Reaction from Plasma-Phase Reaction. *Appl. Catal., B* **2021**, *286*, 119852.
(25) Kim, J.; Go, D. B.; Hicks, J. C. Synergistic Effects of Plasma−Catalyst Interactions for CH 4 Activation. *Phys. Chem. Chem. Phys.* **2017**, *19*, 13010−13021.
(26) Kim, J.; Abbott, M. S.; Go, D. B.; Hicks, J. C. Enhancing C-H Bond Activation of Methane via Temperature-Controlled, Catalyst-Plasma Interactions. *ACS Energy Lett.* **2016**, *1*, 94−99.
(27) Zhang, L.; Heijkers, S.; Wang, W.; Martini, L. M.; Tosi, P.; Yang, D.; Fang, Z.; Bogaerts, A. Dry Reforming of Methane in a Nanosecond Repetitively Pulsed Discharge: Chemical Kinetics Modeling. *Plasma Sources Sci. Technol.* **2022**, *31*, No. 055014.
(28) Gholami, R.; Stere, C.; Chansai, S.; Singhania, A.; Goguet, A.; Hinde, P.; Millington, P.; Hardacre, C. Optimization of Non-Thermal Plasma-Assisted Catalytic Oxidation for Methane Emissions Abatement as an Exhaust Aftertreatment Technology. *Plasma Chem. Plasma Process.* **2022**, *42*, 709−730.
(29) Tu, X.; Whitehead, J. C. Plasma-Catalytic Dry Reforming of Methane in an Atmospheric Dielectric Barrier Discharge: Understanding the Synergistic Effect at Low Temperature. *Appl. Catal., B* **2012**, *125*, 439−448.
(30) Snoeckx, R.; Bogaerts, A. Plasma Technology − a Novel Solution for CO 2 Conversion? *Chem. Soc. Rev.* **2017**, *46*, 5805−5863.
(31) Kozák, T.; Bogaerts, A. Splitting of CO 2 by Vibrational Excitation in Non-Equilibrium Plasmas: A Reaction Kinetics Model. *Plasma Sources Sci. Technol.* **2014**, *23*, No. 045004.
(32) Biswas, A. N.; Winter, L. R.; Loenders, B.; Xie, Z.; Bogaerts, A.; Chen, J. G. Oxygenate Production from Plasma-Activated Reaction of CO 2 and Ethane. *ACS Energy Lett.* **2022**, *7*, 236−241.
(33) Barboun, P.; Mehta, P.; Herrera, F. A.; Go, D. B.; Schneider, W. F.; Hicks, J. C. Distinguishing Plasma Contributions to Catalyst Performance in Plasma-Assisted Ammonia Synthesis. *ACS Sustainable Chem. Eng.* **2019**, *7*, 8621−8630.
(34) Mehta, P.; Barboun, P.; Herrera, F. A.; Kim, J.; Rumbach, P.; Go, D. B.; Hicks, J. C.; Schneider, W. F. Overcoming Ammonia Synthesis Scaling Relations with Plasma-Enabled Catalysis. *Nat. Catal.* **2018**, *1*, 269−275.
(35) Mehta, P.; Barboun, P. M.; Engelmann, Y.; Go, D. B.; Bogaerts, A.; Schneider, W. F.; Hicks, J. C. Plasma-Catalytic Ammonia Synthesis beyond the Equilibrium Limit. *ACS Catal.* **2020**, *10*, 6726−6734.
(36) Wang, W.; Patil, B.; Heijkers, S.; Hessel, V.; Bogaerts, A. Nitrogen Fixation by Gliding Arc Plasma: Better Insight by Chemical Kinetics Modelling. *ChemSusChem* **2017**, *10*, 2145−2157.
(37) Patel, H.; Sharma, R. K.; Kyriakou, V.; Pandiyan, A.; Welzel, S.; van de Sanden, M. C. M.; Tsampas, M. N. Plasma-Activated Electrolysis for Cogeneration of Nitric Oxide and Hydrogen from Water and Nitrogen. *ACS Energy Lett.* **2019**, *4*, 2091−2095.
(38) Sharma, R. K.; Patel, H.; Mushtaq, U.; Kyriakou, V.; Zafeiropoulos, G.; Peeters, F.; Welzel, S.; van de Sanden, M. C. M.; Tsampas, M. N. Plasma Activated Electrochemical Ammonia Synthesis from Nitrogen and Water. *ACS Energy Lett.* **2021**, *6*, 313−319.
(39) Barboun, P. M.; Daemen, L. L.; Waitt, C.; Wu, Z.; Schneider, W. F.; Hicks, J. C. Inelastic Neutron Scattering Observation of Plasma-Promoted Nitrogen Reduction Intermediates on Ni/γ-Al 2 O 3. *ACS Energy Lett.* **2021**, *6*, 2048−2053.
(40) Gibson, E. K.; Stere, C. E.; Curran-McAteer, B.; Jones, W.; Cibin, G.; Gianolio, D.; Goguet, A.; Wells, P. P.; Catlow, C. R. A.; Collier, P.; Hinde, P.; Hardacre, C. Probing the Role of a Non-Thermal Plasma (NTP) in the Hybrid NTP Catalytic Oxidation of Methane. *Angew. Chem., Int Ed.* **2017**, *56*, 9351−9355.
(41) Stere, C. E.; Adress, W.; Burch, R.; Chansai, S.; Goguet, A.; Graham, W. G.; Hardacre, C. Probing a Non-Thermal Plasma Activated Heterogeneously Catalyzed Reaction Using in Situ DRIFTS-MS. *ACS Catal.* **2015**, *5*, 956−964.
(42) Barakat, C.; Gravejat, P.; Guaitella, O.; Thevenet, F.; Rousseau, A. Oxidation of Isopropanol and Acetone Adsorbed on TiO2 under Plasma Generated Ozone Flow: Gas Phase and Adsorbed Species Monitoring. *Appl. Catal., B* **2014**, *147*, 302−313.
(43) Rodrigues, A.; Tatibouët, J.-M.; Fourré, E. Operando DRIFT Spectroscopy Characterization of Intermediate Species on Catalysts Surface in VOC Removal from Air by Non-Thermal Plasma Assisted Catalysis. *Plasma Chem. Plasma Process.* **2016**, *36*, 901−915.
(44) Turan, N.; Barboun, P. M.; Nayak, P. K.; Hicks, J. C.; Go, D. B. Development of a Small-Scale Helical Surface Dielectric Barrier Discharge for Characterizing Plasma−Surface Interfaces. *J. Phys. D: Appl. Phys.* **2020**, *53*, 275201.
(45) Lee, G.; Go, D. B.; O'Brien, C. P. Direct Observation of Plasma-Stimulated Activation of Surface Species Using Multimodal In Situ/Operando Spectroscopy Combining Polarization-Modulation Infrared Reflection-Absorption Spectroscopy, Optical Emission Spectroscopy, and Mass Spectrometry. *ACS Appl. Mater. Interfaces* **2021**, *13*, 56242−56253.
(46) Jo, S.; Lee, D. H.; Kim, K.-T.; Kang, W. S.; Song, Y.-H. Methane Activation Using Kr and Xe in a Dielectric Barrier Discharge Reactor. *Phys. Plasmas* **2014**, *21*, 103504.
(47) Christensen, P. A.; Ali, A. H. B. M.; Mashhadani, Z. T. A. W.; Martin, P. A. A Direct Fourier Transform Infrared Spectroscopic Comparison of the Plasma- and Thermally-Driven Reaction of CO2 at Macor. *Plasma Chem. Plasma Process.* **2018**, *38*, 293−310.
(48) Wu, J.; Xia, Q.; Wang, H.; Li, Z. Catalytic Performance of Plasma Catalysis System with Nickel Oxide Catalysts on Different Supports for Toluene Removal: Effect of Water Vapor. *Appl. Catal., B* **2014**, *156−157*, 265−272.
(49) Nair, S. A.; Nozaki, T.; Okazaki, K. In Situ Fourier Transform Infrared (FTIR) Study of Nonthermal-Plasma-Assisted Methane Oxidative Conversion. *Ind. Eng. Chem. Res.* **2007**, *46*, 3486−3496.
(50) Wang, X.; Wu, J.; Wang, J.; Xiao, H.; Chen, B.; Peng, R.; Fu, M.; Chen, L.; Ye, D.; Wen, W. Methanol Plasma-Catalytic Oxidation over CeO2 Catalysts: Effect of Ceria Morphology and Reaction Mechanism. *Chem. Eng. J.* **2019**, *369*, 233−244.
(51) Lopez, T.; Mangolini, L. On the Nucleation and Crystallization of Nanoparticles in Continuous-Flow Nonthermal Plasma Reactors. *J. Vac. Sci. Technol., B: Nanotechnol. Microelectron.: Mater., Process., Meas., Phenom.* **2014**, *32*, 061802.
(52) Winter, L. R.; Ashford, B.; Hong, J.; Murphy, A. B.; Chen, J. G. Identifying Surface Reaction Intermediates in Plasma Catalytic Ammonia Synthesis. *ACS Catal.* **2020**, *10*, 14763−14774.
(53) Rivallan, M.; Aiello, S.; Thibault-Starzyk, F. Microsecond Time-Resolved Fourier Transform Infrared Analytics in a Low Pressure Glow Discharge Reactor. *Rev. Sci. Instrum.* **2010**, *81*, 103111.
(54) DęBEK, R.; WIERZBICKI, D.; MOTAK, M.; GALVEZ, M. E.; da COSTA, P.; AZZOLINA-JURY, F. Operando FT-IR Study on Basicity Improvement of Ni(Mg, Al)O Hydrotalcite-Derived Catalysts Promoted by Glow Plasma Discharge. *Plasma Science and Technology* **2019**, *21*, No. 045503.
(55) Azzolina-Jury, F.; Thibault-Starzyk, F. Mechanism of Low Pressure Plasma-Assisted CO2 Hydrogenation Over Ni-USY by Microsecond Time-Resolved FTIR Spectroscopy. *Top. Catal.* **2017**, *60*, 1709−1721.
(56) Azzolina-Jury, F.; Bento, D.; Henriques, C.; Thibault-Starzyk, F. Chemical Engineering Aspects of Plasma-Assisted CO 2 Hydrogenation over Nickel Zeolites under Partial Vacuum. *J. CO2 Util.* **2017**, *22*, 97−109.
(57) Radmilović-Radjenović, M.; Radjenović, B.; Matejčik, Š.; Klas, M. The Breakdown Phenomena in Micrometer Scale Direct-Current Gas Discharges. *Plasma Chem. Plasma Process.* **2014**, *34*, 55−64.

https://doi.org/10.1021/acsengineeringau.2c00026
ACS Eng. Au 2022, 2, 535−546

(58) Schlögl, R. Heterogeneous Catalysis. *Angew. Chem., Int. Ed.* **2015**, *54*, 3465−3520.
(59) Cybulskis, V. J.; Harris, J. W.; Zvinevich, Y.; Ribeiro, F. H.; Gounder, R. A Transmission Infrared Cell Design for Temperature-Controlled Adsorption and Reactivity Studies on Heterogeneous Catalysts. *Rev. Sci. Instrum.* **2016**, *87*, 103101.
(60) Teschke, M.; Kedzierski, J.; Finantu-Dinu, E. G.; Korzec, D.; Engemann, J. High-Speed Photographs of a Dielectric Barrier Atmospheric Pressure Plasma Jet. *IEEE Trans. Plasma Sci.* **2005**, *33*, 310−311.
(61) Mears, D. E. Tests for Transport Limitations in Experimental Catalytic Reactors. *Ind. Eng. Chem. Process Des. Dev.* **1971**, *10*, 541−547.
(62) Zhao, D.; Feng, J.; Huo, Q.; Melosh, N.; Fredrickson, G. H.; Chmelka, B. F.; Stucky, G. D. Triblock Copolymer Syntheses of Mesoporous Silica with Periodic 50 to 300 Angstrom Pores. *Science* **1998**, *279*, 548−552.
(63) Hicks, J. C.; Drese, J. H.; Fauth, D. J.; Gray, M. L.; Qi, G.; Jones, C. W. Designing Adsorbents for CO2 Capture from Flue Gas-Hyperbranched Aminosilicas Capable of Capturing CO 2 Reversibly. *J. Am. Chem. Soc.* **2008**, *130*, 2902−2903.
(64) Peeters, F.; Butterworth, T. Electrical Diagnostics of Dielectric Barrier Discharges. In *Atmospheric Pressure Plasma - from Diagnostics to Applications*; IntechOpen, 2019, 1−27, DOI: 10.5772/intechopen.80433.
(65) McKittrick, M. W.; Jones, C. W. Toward Single-Site Functional MaterialsPreparation of Amine-Functionalized Surfaces Exhibiting Site-Isolated Behavior. *Chem. Mater.* **2003**, *15*, 1132−1139.
(66) Hicks, J. C.; Jones, C. W. Controlling the Density of Amine Sites on Silica Surfaces Using Benzyl Spacers. *Langmuir* **2006**, *22*, 2676−2681.
(67) Hicks, J. C.; Dabestani, R.; Buchanan, A. C.; Jones, C. W. Assessing Site-Isolation of Amine Groups on Aminopropyl-Functionalized SBA-15 Silica Materials via Spectroscopic and Reactivity Probes. *Inorg. Chim. Acta* **2008**, *361*, 3024−3032.
(68) Chen, J.-Y.; Brunelli, N. A. Investigating the Impact of Microporosity of Aminosilica Catalysts in Aldol Condensation Reactions for Biomass Upgrading of 5-Hydroxymethylfurfural and Furfuraldehyde to Fuels. *Energy Fuels* **2021**, *35*, 14885−14893.
(69) Deshpande, N.; Cho, E. H.; Spanos, A. P.; Lin, L.-C.; Brunelli, N. A. Tuning Molecular Structure of Tertiary Amine Catalysts for Glucose Isomerization. *J. Catal.* **2019**, *372*, 119−127.
(70) McCurry, D. L.; Quay, A. N.; Mitch, W. A. Ozone Promotes Chloropicrin Formation by Oxidizing Amines to Nitro Compounds. *Environ. Sci. Technol.* **2016**, *50*, 1209−1217.
(71) Bailey, P. S.; Keller, J. E. Ozonation of Amines. III. Tert-Butylamine. *J. Org. Chem.* **1968**, *33*, 2680−2684.
(72) Lim, S.; McArdell, C. S.; von Gunten, U. Reactions of Aliphatic Amines with Ozone: Kinetics and Mechanisms. *Water Res.* **2019**, *157*, 514−528.
(73) Skrotzki, E. A.; Vandavasi, J. K.; Newman, S. G. Ozone-Mediated Amine Oxidation and Beyond: A Solvent-Free, Flow-Chemistry Approach. *J. Org. Chem.* **2021**, *86*, 14169−14176.
(74) Bollini, P.; Choi, S.; Drese, J. H.; Jones, C. W. Oxidative Degradation of Aminosilica Adsorbents Relevant to Postcombustion CO 2 Capture. *Energy Fuels* **2011**, *25*, 2416−2425.
(75) Lin-Vien, D.; Colthup, N. B.; Fateley, W. G.; Grasselli, J. G. Compounds Containing −NH2, −NHR, and −NR2 Groups. In *The Handbook of Infrared and Raman Characteristic Frequencies of Organic Molecules*; Elsevier, 1991; pp. 155−178, DOI: 10.1016/B978-0-08-057116-4.50016-X.
(76) Lin-Vien, D.; Colthup, N. B.; Fateley, W. G.; Grasselli, J. G. The Nitro Group. In *The Handbook of Infrared and Raman Characteristic Frequencies of Organic Molecules*; Elsevier, 1991; pp. 179−189, DOI: 10.1016/B978-0-08-057116-4.50017-1.
(77) Lin-Vien, D.; Colthup, N. B.; Fateley, W. G.; Grasselli, J.; G., Alkanes. In *The Handbook of Infrared and Raman Characteristic Frequencies of Organic Molecules*; Elsevier, 1991; pp. 9−28, DOI: 10.1016/B978-0-08-057116-4.50008-0.
(78) Lin-Vien, D.; Colthup, N. B.; Fateley, W. G.; Grasselli, J. G. Selected Infrared and Raman Spectra from the Sadtler Research Laboratories, Division of Bio-Rad Laboratories, Inc. for Compounds with Structures Discussed In. In *The Handbook of Infrared and Raman Characteristic Frequencies of Organic Molecules*; Elsevier, 1991; pp. 307−422, DOI: 10.1016/B978-0-08-057116-4.50024-9.
(79) Higuchi, S.; Kuno, E.; Tanaka, S.; Kamada, H. Some Considerations about the Substituent Effect on the Infrared Absorption Intensities of Symmetric Stretching and Bending Vibrations of Methyl Group. *Spectrochim. Acta, Part A* **1972**, *28*, 1335−1346.
(80) Lin-Vien, D.; Colthup, N. B.; Fateley, W. G.; Grasselli, J. G. Compounds Containing the Carbonyl Group. In *The Handbook of Infrared and Raman Characteristic Frequencies of Organic Molecules*; Elsevier, 1991; pp. 117−154, DOI: 10.1016/B978-0-08-057116-4.50015-8.
(81) Lin-Vien, D.; Colthup, N. B.; Fateley, W. G.; Grasselli, J. G. Double Bonds Containing Nitrogen Atoms. In *The Handbook of Infrared and Raman Characteristic Frequencies of Organic Molecules*; Elsevier, 1991; pp. 191−211, DOI: 10.1016/B978-0-08-057116-4.50018-3.
(82) NIST Mass Spectrometry Data Center, W. E. W. director. Infrared Spectra. In *NIST Chemistry WebBook*, NIST Standard Reference Database Number 69; Linstrom, P. J., Mallard, W. G., Eds.; National Institute of Standards and Technology: Gaithersburg MD, 20899, DOI: 10.18434/T4D303.
(83) Poenariu, V.; Wertheimer, M. R.; Bartnikas, R. Spectroscopic Diagnostics of Atmospheric Pressure Helium Dielectric Barrier Discharges in Divergent Fields. *Plasma Processes Polym.* **2006**, *3*, 17−29.
(84) Mouele, E. S. M.; Tijani, J. O.; Badmus, K. O.; Pereao, O.; Babajide, O.; Fatoba, O. O.; Zhang, C.; Shao, T.; Sosnin, E.; Tarasenko, V.; Laatikainen, K.; Petrik, L. F. A Critical Review on Ozone and Co-Species, Generation and Reaction Mechanisms in Plasma Induced by Dielectric Barrier Discharge Technologies for Wastewater Remediation. *Journal of Environmental Chemical Engineering* **2021**, *9*, 105758.
(85) Biloiu, C.; Sun, X.; Harvey, Z.; Scime, E. An Alternative Method for Gas Temperature Determination in Nitrogen Plasmas: Fits of the Bands of the First Positive System (B Π3g→A Σ3u+). *J. Appl. Phys.* **2007**, *101*, No. 073303.
(86) Britun, N.; Gaillard, M.; Ricard, A.; Kim, Y. M.; Kim, K. S.; Han, J. G. Determination of the Vibrational, Rotational and Electron Temperatures in N 2 and Ar−N 2 Rf Discharge. *J. Phys. D: Appl. Phys.* **2007**, *40*, 1022−1029.
(87) Poncin-Epaillard, F.; Legeay, G. Surface Engineering of Biomaterials with Plasma Techniques. *J. Biomater. Sci., Polym. Ed.* **2003**, *14*, 1005−1028.
(88) Ma, H.; Sharma, R. K.; Welzel, S.; van de Sanden, M. C. M.; Tsampas, M. N.; Schneider, W. F. Observation and Rationalization of Nitrogen Oxidation Enabled Only by Coupled Plasma and Catalyst. *Nat. Commun.* **2022**, *13*, 402.
(89) Patil, B. S.; Wang, Q.; Hessel, V.; Lang, J. Plasma N2-Fixation: 1900−2014. *Catal. Today* **2015**, *256*, 49−66.
(90) Chao, C.-C.; Lunsford, J. H. Infrared Studies of the Disproportionation Reaction of Nitric Oxide on Y-Type Zeolites. *J. Am. Chem. Soc.* **1971**, *93*, 71−77.
(91) Djonev, B.; Tsyntsarski, B.; Klissurski, D.; Konstantin Hadjiivanov. Konstantin Hadjiivanov, and. IR Spectroscopic Study of NOxadsorption and NOx−O2coadsorption on Co2+/SiO2catalysts. *J. Chem. Soc., Faraday Trans.* **1997**, *93*, 4055−4063.
(92) Uytterhoeven, J. B.; Christner, L. G.; Hall, W. K. Studies of the Hydrogen Held by Solids. VIII. The Decationated Zeolites. *J. Phys. Chem.* **1965**, *69*, 2117−2126.
(93) Li, W. T.; Boswell, R.; Samoc, M.; Samoc, A.; Wang, R. P. The Effect of Defects on the Optical Nonlinearity of Thermally Poled SiOx Thin Films. *Thin Solid Films* **2008**, *516*, 5474−5477.
(94) Gerhard, C.; Letien, E.; Cressent, T.; Hofmann, M. Inline Monitoring of Hydrogenous Plasma-Induced Defect Formation

within Fused Silica via Plasma Emission Spectroscopy. *Appl. Phys. A* **2020**, *126*, 165.
(95) Devine, R. A. B.; Leray, J.; Margail, J. Ultraviolet Radiation Induced Defect Creation in Buried SiO 2 Layers. *Appl. Phys. Lett.* **1991**, *59*, 2275−2277.
(96) Hadjiivanov, K. I. Identification of Neutral and Charged N x O y Surface Species by IR Spectroscopy. *Catal. Rev.* **2000**, *42*, 71−144.
(97) Levoguer, C. L.; Nix, R. M. A Study of the Adsorption of NO on a Polycrystalline Pt Foil by FT-RAIRS. *Surf. Sci.* **1996**, *365*, 672−682.
(98) Banholzer, W. F.; Masel, R. I. A Reflection-Absorption Infrared Study of Carbon Monoxide and Nitric Oxide Adsorption on Platinum (100). *Surf. Sci.* **1984**, *137*, 339−360.
(99) Gorte, R. J.; Gland, J. L. Nitric Oxide Adsorption on the Pt(110) Surface. *Surf. Sci.* **1981**, *102*, 348−358.
(100) Hayden, B. E. An Infra-Red Reflection Absorption Study of the Adsorption of NO on Pt(111). *Surf. Sci.* **1983**, *131*, 419−432.

https://doi.org/10.1021/acsengineeringau.2c00026
ACS Eng. Au 2022, 2, 535−546